

Imaging the exploding converter with elastic propagators

Brad Artman, Igor Podladtchikov, Alex Goertz, Brian Steiner, Erik Saenger

Submitted to EAGE Amsterdam 2009

Summary

Since the Earth is elastic, it is worth the computational burden to process multicomponent data for elastic phenomena with fully coupled time-domain wave-equation propagators. At every time sample in the back-propagated model domain, the complete wave field can be decomposed exactly into compressional and shear wave components by simple spatial derivatives. Then, physically significant images are extracted from extrapolated hyper-cubes by applying appropriate imaging conditions. For subsurface source location, the imaging condition required is the correlation of P and S energy since only at the source location are the two events collocated. The impulse response of the algorithm is anti-symmetric in physical space and can be enhanced through post-processing with a spatial derivative or integral.

Multicomponent reflector imaging

Shot record migration is explained as the process of locating the convergence of the two travel paths that compose the two-way time delays recorded in active seismic data (Claerbout, 1971). The main idea is to image reflections by separately modeling the propagation of the source and receiver wave fields and finding the location where they are coincident. Coincidence is found by extracting the zero lag of the cross correlation of the two wave fields at depth. The topic, reverse-time migration (RTM), is further elucidated in Levin (1984) for acoustic time-domain propagators specifically.

An extension of the “exploding reflector” concept (Claerbout, 1985), or the “exploding (mode) converter,” can be used to understand imaging schemes for migrating compressional to shear (P-S) converted reflections with separate acoustic propagators. Historically, acquisition plane processing has been relied on for wave field decomposition (Zhe and Greenhalgh, 1997; Dellinger et al., 2001). Coupling between the shear and compressional wave fields is introduced in the imaging condition via a correlation of the two wave fields. This is effectively a single-scattering representation of the complete wave equation.

With a modest increase in computational burden, the full elastic solution to the wave equation can be implemented as opposed to the far-field acoustic approximations routinely utilized. So doing removes the need for approximate surface processing of the raw data to separate P and S energy within the records. However, this introduces the need for wave-field decomposition during the imaging stage. Performing the decomposition in the model domain after extrapolation ensures a regular and complete domain that does not require approximations for the vertical derivative (Huang and Milkereit, 2007). Fortunately, only two simple vector identities are needed to separate P and S energy exactly since the displacement wave field, $\mathbf{u}(\mathbf{x}, t)$, can be described as the sum of Helmholtz potentials (HP).

Capitalizing on the facts that the curl of the irrotational HP is zero and the divergence of the solenoidal HP is zero, the compressional, E_p , and shear kinetic energies E_s , are (Morse and Feshbach, 1953)

$$E_p = P^2 = (\lambda + 2\mu)(\nabla \cdot \mathbf{u})^2 \quad (1)$$

$$E_s = S^2 = \mu(-\nabla \times \mathbf{u})^2, \quad (2)$$

where the Lamé coefficients λ and μ scale the amplitude of the results. The wave fields P and S have preserved sign information that captures the relative energy amplitudes within the two propagation modes (Dougherty and Stephen, 1988). The correlation type combination of the wave field components P and S to image the mode-converted reflections in active seismic data is (Wapenaar et al., 1987; Yan and Sava, 2008)

$$I_{ps}(\mathbf{x}) = \sum_t P_d(\mathbf{x}, t) S_u(\mathbf{x}, t), \quad (3)$$

where subscripts d and u refer to extraction of the HP's from the down-going and up-coming wave fields.

Imaging forward scatterers

Shragge et al. (2006) introduced industry-style (shot-domain) imaging with teleseismic earthquake sources. Following the Kirchhoff-based work of Bostock et al. (2001), they proposed imaging conditions for reflections and mode conversions for the depth domain. Based on scalar propagators, those results still require accurate earthquake arrival parameters to decompose the data into P- and S-wave components at the acquisition plane.

More importantly, Shragge et al. (2006) introduced imaging forward scattered mode conversions by simply changing the causality of the source propagation. The forward scattering (one-way) P to S imaging condition can also be interpreted as the location of an oriented source, which leads to concept of imaging an actual “explosion” instead of the “exploding reflector.”

An oriented subsurface source instigates both P and S waves that separate in the far field where they are recorded. By finding the model coordinates where the P and S energy is collocated, we identify the source

location. Using the vector identities provided by equations 1 and 2 eliminates the need to characterize the source and process the data before imaging.

Single travel path imaging

The time-reverse modeling (TRM) algorithm was developed for locating sources within the domain (Fink, 1999; Gajewski and Tessmer, 2005). The method is suited for locating earthquakes, microseisms, or tremor sources. Defining an appropriate imaging condition for TRM has historically been a challenge because there may be no knowledge of absolute time. Steiner et al. (2008) uses the maximum particle velocity over all time, which is shown to be similar to the zero-lag of the autocorrelated wave field (ie. illumination map) in Artman and Podladtchikov (2009). The difference between TRM and RTM is the lack of a known source wave field for TRM. Otherwise, data are treated in the same manner: reversed in time and used as source functions at the acquisition plane. TRM can be implemented for borehole geometries as well, though the examples herein will use surface acquisition geometries.

We propose using the P-S elastic imaging condition for imaging subsurface sources which exploits the fact that the P and S-waves produced by an oriented source propagate at different speeds. The model domain location at which these wave types are both at time zero after reverse propagation is the location of the source. Therefore, the TRM imaging condition for locating body wave generators is

$$I_b(\mathbf{x}) = \sum_t P_u(\mathbf{x}, t) S_u(\mathbf{x}, t). \quad (4)$$

Subscript b refers to the assumption P and S body waves are produced by the source. Note the similarity to equation 3 with the important difference that both potentials are extracted from the up-coming wave field. Secondary sources (diffractors) are sources within this context and are also imaged.

The global algorithm is a chain of: propagation, decomposition, and correlation. A time-domain finite-difference solution to the elastic wave equation is used for propagation. Multicomponent time-reversed data are source functions for the outer time loop. Wave field decomposition and correlations are performed for each time step. Because only the zero lag of the correlations are required, the image is simply calculated by accumulating the product of wave fields at every extrapolation step.

Figure 1 shows the collapse of energy from a source at depth recorded at the surface via reverse propagation of the elastic wave field. The panels are all extracted from the extrapolation time axis at the initiation time of a vertical point source. Panel a is the sum of the squares of the Cartesian displacement components. Panels b and c are the P and S-wave potentials respectively. The source is located at the maximum amplitude of panel a and at the zero crossings in the center of panels b and c. Longer wavelengths are seen on the P image due to faster propagation velocity. The extra events on panel b are the limited aperture artifacts. The hyperbola on panel c is the P-S conversion at the free surface. The linear events are nonphysical artifacts associated with using the data as displacement sources.

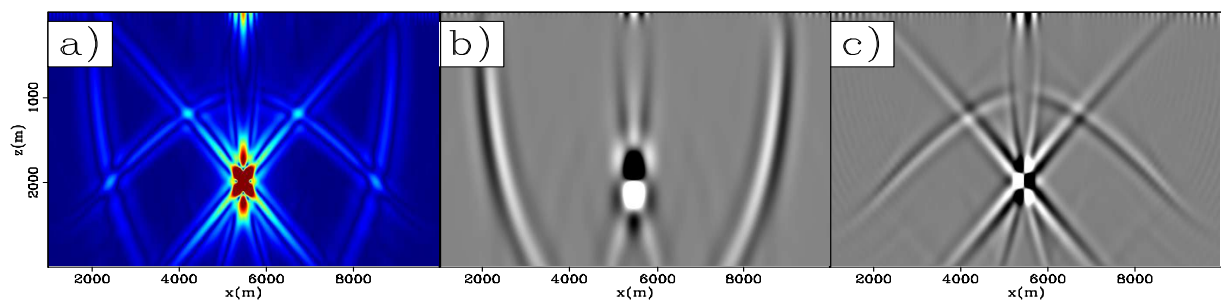


Figure 1 Absolute particle velocity, P and S wave fields after after reverse propagating to the depth of a vertical point source.

Figure 2 shows the zero lag of the autocorrelations of P and S energy and their cross correlation after reverse propagating the forward modeled data. While the autocorrelations are strictly positive, the

correlation of the P and S wave fields has zero mean. The source location in panel c is at the location of a zero crossing, thereby having an amplitude identical (or similar) to most of the rest of the domain. The anti-symmetric clover-leaf pattern surrounding the source identifies its location. For unknown source functions, computing all three images will provide polarization information about the source function as well as location.

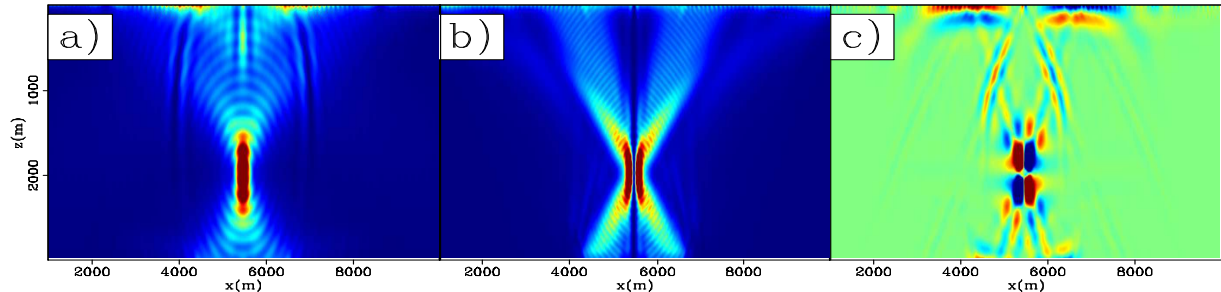


Figure 2 Auto and cross-correlations of component wave fields imaging a vertical point source by TRM with an elastic propagator. Panels a, b and c are PP, SS, and PS respectively.

The asymmetry revealed in the impulse response of the mode cross-correlation imaging condition in Figure 2c suggests simple post-processing to identify the source position with a energy anomaly instead of the multidimensional zero crossing seen in the image. The spatial integral or derivative of the image in panel c will provide a $\pm 90^\circ$ phase roll in the image that will locate the source with a maximum.

Figure 3a shows a realistic velocity model used to forward model a source location experiment. Constant V_p/V_s ratio and density were used. The receiver stations used for TRM are indicated by the circles at the top of panels b and c. Panel b is the TRM image with correlation imaging condition of the P and S wave fields (equation 4). The modeled data were produced with a swarm of randomly triggered point sources with Ricker wavelet time functions, central frequency 4.5 Hz. The complexities of irregular acquisition geometry, $V(x, z)$, and simultaneously imaging many sources introduce cross-talk artifacts. However, panel b shows a feature resembling the antisymmetric cloverleaf seen in the impulse response image in Figure 1. Panel c is the integration of panel b with the source locations overlain.

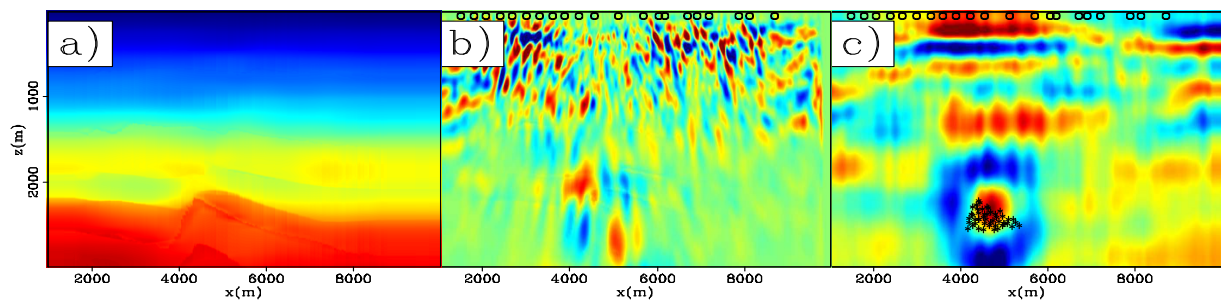


Figure 3 Velocity model and P-S body-wave TRM images before (b) and after (c) applying spatial integral. Irregular data acquisition was modeled as well as a swarm of random sources imaged together.

Conclusions

When recording the full wave field in any geophysical experiment, it is logical to use fully elastic propagators for a migration or focusing algorithm. Especially in the case of event location, the TRM algorithm benefits from elastic propagators since sufficient characterization of the source may be impossible for wave field decomposition at the acquisition plane. This is particularly important for sources that are not transient in nature or compact in time.

We use the chain of elastic propagation, wave field decomposition, and correlation imaging (defined as migration) to image source locations. In this application the critical time differences used for imaging are extracted from the time delay between P and S-wave travel paths. The algorithm is both a refinement

of time-reverse modeling and a migration, which more completely links the two as suggested in Artman and Podladtchikov (2009).

Physical interpretation of the back-propagated data is extracted by applying imaging conditions designed to extract particular kinematic events within the data. For the case of locating subsurface sources, the imaging condition we have selected is the correlation of the P and S-wave energy. In the forward scattering (one-way travel path) observation of non-explosive sources, the energy partition between compressional and shear waves is only collocated at the physical origin of the source. The methodology is sufficiently robust to tolerate irregular acquisition geometry and multiple sources in the wave field.

REFERENCES

- Artman, B. and Podladtchikov, I. [2009] Imaging conditions for time-reverse acoustics. In: *Passive seismic workshop, Limassol Cyprus*. EAGE.
- Bostock, M.G., Rondenay, S., and Shragge, J.C. [2001] Multi-parameter two-dimensional inversion of scattered teleseismic body waves, 1. Theory for oblique incidence. *J. Geophys. Res.*, **106**, 30771–30782.
- Claerbout, J.F. [1971] Toward a unified theory of reflector mapping. *Geophysics*, **36**(03), 467–481.
- Claerbout, J. [1985] *Imaging the Earth's interior*. Blackwell Scientific Publications.
- Dellinger, J.A., Nolte, B., and Etgen, J.T. [2001] Alford rotation, ray theory, and crossed-dipole geometry. *Geophysics*, **66**(2), 637–647.
- Dougherty, M.E. and Stephen, R.A. [1988] Seismic energy partitioning and scattering in laterally heterogeneous ocean crust. *Pure and Applied Geophysics*, **128**(1/2), 195–229.
- Fink, M. [1999] Time-reversed acoustics. *Scientific American*, **November**, 67–73.
- Gajewski, D. and Tessmer, E. [2005] Reverse modelling for seismic event characterization. *Geophys. J. Int.*, **163**, 276–284.
- Huang, J. and Milkereit, B. [2007] Wave-equation-based separation of p- and s-wave modes. *SEG Technical Program Expanded Abstracts*, **26**(1), 2135–2139.
- Levin, S.A. [1984] Principle of reverse-time migration. *Geophysics*, **49**(5), 581–583.
- Morse, P.M. and Feshbach, H. [1953] *Methods of Theoretical Physics*. McGraw-Hill Book Company. New York.
- Shragge, J.C., B. Artman, and C. Wilson [2006] Teleseismic shot-profile migration. *Geophysics*, **71**(4), SI221–SI229.
- Steiner, B., Saenger, E.H., and Schmallholz, S.M. [2008] Time reverse modeling of low-frequency microtremors: Application to hydrocarbon reservoir localization. *Geophysical Research Letters*, **35**, L03307.
- Wapenaar, C.P.A., Kinneging, N.A., and Berkhout, A.J. [1987] Principle of prestack migration based on the full elastic two-way wave equation. *Geophysics*, **52**(2), 151–173.
- Yan, J. and Sava, P. [2008] Isotropic angle-domain elastic reverse-time migration. *Geophysics*, **73**(6), S229–S239.
- Zhe, J. and Greenhalgh, S.A. [1997] Prestack multicomponent migration. *Geophysics*, **62**(2), 598–613.